Organic & Biomolecular Chemistry

ROYAL SOCIETY OF CHEMISTRY

PAPER

View Article Online
View Journal | View Issue



Cite this: *Org. Biomol. Chem.*, 2026, **24**, 2683

# Dynamic N→B coordination and anion-selective turn-on fluorescence in oxadiazole-functionalized organoboranes

Jonas D. W. Schepper,[c] Andreas Orthaber [b] and Frank Pammer *[a]

A versatile route for the preparation of chemically and electronically diverse $Mes_2BPh$-based boranes (Mes = mesityl, 2,4,6-trimethylphenyl) is presented that allows the conversion of tetrazolyl rings in a common borane precursor (**2H**) into boranes bearing variously substituted oxadiazolyl groups. A series of eight boranes (**4a–4h**) was prepared with functional groups on the 5-position of the oxadiazole ranging from electron donating (**4a**: 4-Me-phenyl, **4b**: 4-MeO-phenyl, *etc.*) to strongly electron withdrawing (**4d**: 4-$O_2N$-phenyl, **4e**: 3,5-bis($CF_3$)-phenyl, **4h**: $CF_3$) and also including a bifunctionalized example bearing two $Mes_2B$ moieties (**4g**). A full characterization study of the optical, electrochemical and electronic properties, both experimentally and by DFT calculations, was carried out. Our investigation shows that the boranes exhibit dynamic equilibria between ***closed*** intramolecularly N→B-coordinated and ***open*** non-coordinated conformers, as indicated by variable temperature NMR, $^{11}B$ NMR and anion binding studies with $F^-$ and $CN^-$. The anion binding studies reveal substantial differences in the fluorescence response of the compounds ranging from differing degrees of quenching to fluorescence shifts (**4g**) and enhanced emission (**4c**) (4-OMe-phenyl). These results show that this synthetic strategy allows easy creation of a series of compounds with incrementally varied optical properties and Lewis acidities.

Received 22nd December 2025,
Accepted 23rd February 2026

DOI: 10.1039/d5ob01979f

rsc.li/obc



## Introduction

The exploitation of intramolecular dynamic processes is of increasing interest in current chemical research.[1,2] For instance, hemilabile coordination of chelating ligands to transition metals has been recognized as crucial for many catalytic processes[3] and was exploited in the development of sensing applications.[4]

One of the greatest strengths of organic materials is their large structural variety and the resulting broad range of physical and electronic properties. In this context, the introduction of main group elements into organic scaffolds is being intensively investigated to access new structural motifs and to exploit unusual electronic effects.[5] The introduction of boron[6–14] has attracted particular interest in this regard as it can be incorporated in either the tri-[7,15–17] or tetracoordinate[18–26] form, which gives rise to different electronic and chemical properties.

Tricoordinate boron centers in pendant groups[17,27–32] or embedded within π-systems[33–40] lead to a lowering of the Lowest Unoccupied Molecular Orbital (LUMO) and hence increased electron affinity, due to conjugation with their $p_z$-orbital. Likewise, tricoordinate boranes with tailored Lewis acidity are of great interest as catalysts and chemical sensors.[41–43] Compounds featuring intramolecular N,$C^2$-chelated tetracoordinate boron (N→B-ladders)[26,44–49] also exhibit increased electron affinity and have therefore been considered as electron-transporting (n-type) materials.[18–26,50] Recently, N→B-ladders have attracted growing interest due to their promising results in organic light emitting devices,[51] n-channel organic field effect transistors,[52] and organic photovoltaic cells.[23,24,53] The N→B-ladder motif has also been exploited for generating compounds with helical topology.[54–56]

An intriguing feature of ladder boranes is that they can exist in dynamic equilibria between ***closed*** D→B-coordinated (D = N, O, P) and ***open*** non-coordinated conformers (Scheme 1). This behavior is observed, for instance, when the donor atom is part of a heterocycle with low basicity, such as a triazole[57,58] or a tetrazole,[59] and also in sterically congested compounds[60] or when strained 4-,[61,62] 7-[63] or 8-membered[64,65] ring systems are formed. Similarly, reduced Lewis acidity at the boron center[66] and weak Lewis bases such as ethers[67] or carbonyl moieties[68] facilitate dynamic coordination.

[a]*Helmholtz Institute Ulm, Karlsruhe Institute for Technology, Helmholtzstrasse 11, 89081 Ulm, Germany. E-mail: frank.pammer@kit.edu*
[b]*Department of Chemistry – Ångström Laboratories, Uppsala University, BOX 523, 75120 Uppsala, Sweden. E-mail: andreas.orthaber@kemi.uu.se*
[c]*Institute of Organic Chemistry II and Advanced Materials, Ulm University, Albert-Einstein-Allee 11, 89081 Ulm, Germany*

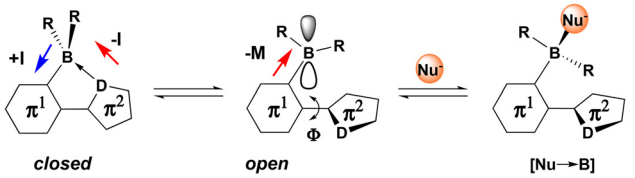


**Scheme 1** Conformers of labile coordinated ladder boranes. D: Lewis basic donor atoms: N, O, P.

Labile D→B-coordination can have a strong influence on the electronic properties of a given π-system (Scheme 1). In the ***closed*** D→B-conformation, the π-system is planarized ($\Phi \approx 0°$), and conjugation along the backbone is more effective, while the tetracoordinate boron center acts as an electron-rich inductive donor (+I) towards the $\pi^1$-ring systems. At the same time, the D→B-interaction exerts an electron withdrawing effect (−I) onto the donor atom (D) in the $\pi^2$-ring. In the ***open*** conformation, the empty $p_z$-orbital on boron exerts a strong electron withdrawing mesomeric effect (−M) on the π-system, while conjugation along the backbone is less efficient due to increased torsion ($|\Phi| \gg 0°$). Furthermore, in the ***open*** conformation, the boron center can act as a Lewis acid that can bind nucleophiles ([Nu→B]). This latter property of organoboranes has been exploited to develop *e.g.* chemical sensors for various anions[69,70] and to develop fluorescent dyes with extreme Stokes' shifts.[67]

A key limitation in the exploration of organoboranes is the limited choice of methods for their preparation. The most commonly used methods are step-wise metalation[26,30,34] and electrophilic C–H-borylation.[71,72] Hydroboration of suitable substrates can also yield a broad range of N→B-heterocycles.[24,73–79]

In this report, we demonstrate a versatile synthetic route to compounds capable of labile intramolecular N→B-coordination that builds on our previous work on this topic.

We developed strategies for the synthesis of N→B-heterocycles by building up the N-heterocyclic component through cycloaddition reactions. We found that 1,3-dipolar [3 + 2] azide–alkyne cycloaddition,[57,58] [3 + 2] azide–nitrile cycloaddition,[59] and cobalt-mediated [2 + 2 + 2] cycloaddition between nitriles and alkynes[80] are highly efficient tools for the preparation of electronically and structurally diverse N→B-ladder boranes.

In a recent paper on the synthesis of tetrazole containing organoboranes (Scheme 2A),[59] we reported the preparation of phenyltetrazole **2H**, which proved to be a versatile starting material for the syntheses described herein: in this paper, we explored the scope of tetrazole/oxadiazole conversion for the preparation of a broad range of organoboranes with variable electronic properties (Schemes 2B and 4).

The tetrazole ring in **2H** can be acylated to give *N*-acyl-tetrazoles (**3**), which then rearrange into 2,5-disubstituted 1,3,4-oxadiazoles (**4**) with the concurrent loss of molecular nitrogen due to their thermal instability (Scheme 3).[81,82] 1,3,4-Oxadiazoles have a wide range of applications in pharmaceuticals[83] and as

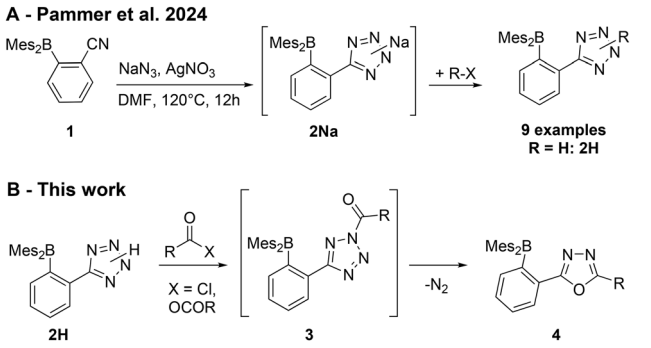


**Scheme 2** (A) Preparation of tetrazole-functionalized organoboranes[81] and (B) their conversion into 1,3,4-oxadiazoles.

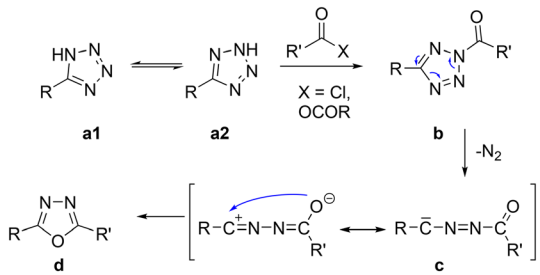


**Scheme 3** Mechanism for the conversion of tetrazoles into 1,3,4-oxadiazoles.[81]

semiconductors in organic light-emitting diodes (OLEDs).[84,85] Examples of 1,3,4-oxadiazole-based ladder boranes have been reported[86,87] that exhibit thermally activated delayed fluorescence (TADF)[87] and can serve as blue-emitter materials in OLEDs with high electron mobilities.[86]

A significant advance over previously reported N→B-ladders is the full conjugation across the heterocycle in the systems reported herein (Chart 1A, 'type 4'). In triazole-[57,58] (Chart 1B, 'type 5') and tetrazole-[59] (Chart 1C, 'type 6') containing N→B-ladders, substituents could only be introduced on a saturated,

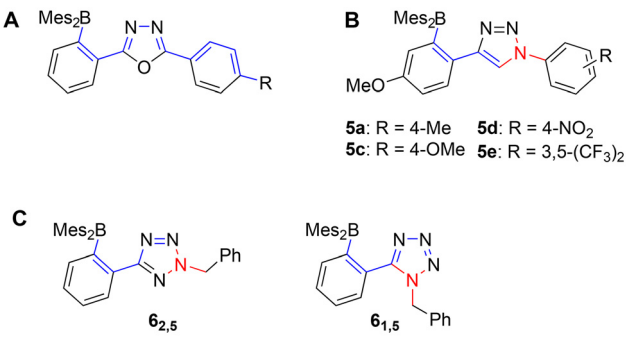


**Chart 1** Conjugation across the heterocycle in different N→B-ladder boranes. — : Maximum conjugated pathway starting at boron. (A) Oxadiazoles in this work. (B) Triazoles adopted from ref. 57 (see also ref. 58). (C) Tetrazoles adopted from ref. 69. N— : Conjugation breaking atoms/bonds. R: functional groups.

conjugation-breaking ring nitrogen (N—). Unsaturated peripheral substituents therefore invariably experience only limited (cross-) conjugation in the π-system. In the case of tetrazoles (C), the synthesis only allowed the introduction of alkyl-substituents on the ring nitrogen, which preempts extension of the conjugated system. Due to a lack of boranes with directly comparable π-systems, the experimental data only weakly reflect the improved conjugation in type 4 *vs.* type 5/6, as will be discussed further on.

## Results and discussion

### Synthesis and structure

The oxadiazole synthesis was tested and optimized by acylating tetrazole **2H**[59] with *p*-toluoyl chloride (→**3a**) at ambient temperature and subsequent conversion into 1,3,4-oxadiazole **4a** (Table 1) at different temperatures. Upon addition of *p*-toluoyl chloride to a suspension of **2H** in toluene, the reaction mixture immediately turned intensely yellow in color attributed to the formation of acyltetrazole **3a**. Upon heating, foaming and gas evolution could be observed as deazotation set in and the yellow coloring steadily faded. When the deazotation reaction was carried out at 110 °C, the corresponding oxadiazole **4a** could be isolated in a yield of 35% after purification by column chromatography (Table 1). Lower (90 °C) and higher (130 °C) reaction temperatures gave significantly lower yields of 15% and 13%, respectively (see Table 1). To increase the yield, different bases ($NEt_3$ and $K_2CO_3$) were added to trap the liberated HCl. The use of $NEt_3$ did not result in a substantial increase in yield, but the addition of $K_2CO_3$ allowed near quantitative isolation (95%) of **4a**. A comparison of NMR experiments with and without the addition of $K_2CO_3$ (see Fig. S1A in the SI) showed that mesitylene (Mes-H) was formed after heating to 110 °C when no base was present, likely due to protolysis of the B-Mes bonds in **2H**, **3** or **4** by HCl (see Fig. 1). In contrast, Mes-H-formation could not be observed when $K_2CO_3$ was added, since the base effectively captured the acid (see Fig. S1A in the SI). The protolysis would initially produce boryl-chloride **7** (Fig. 1) which could react further to the more chemically robust borinic acids (**8**) through reaction with trace moisture or $OH^-$ from the glass of the reaction vessel or during workup. This was confirmed in the synthesis of compound **4b**, with the isolation of **8b** (see Fig. 1) when no basic additive was used.

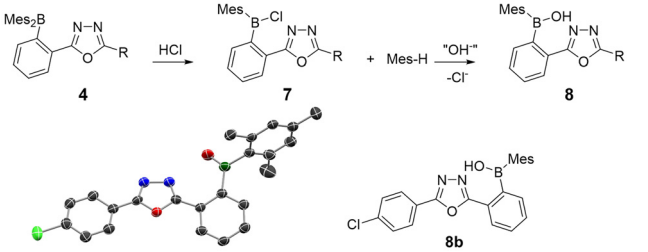


**Fig. 1** Top: Example of the formation of borinic acids **8**. Bottom: Crystal structure of borinic acid **8b**, which was crystallized during the workup of compound **4b**; ellipsoids are shown with 50% probability; hydrogen atoms have been omitted for clarity.

With the reaction conditions optimized as described above, seven other 5-aryl-substituted 1,3,4-oxadiazoles could be synthesized using commercially available acid chlorides (see Scheme 4). Oxadiazoles **4a** to **4f** were isolated in very good yields of 84–99%. The diborylated compound **4g**, which is accessible by using terephthalic acid dichloride as an acylating agent, could be isolated in only 36% yield. Both electron rich (**4a**, **4c**) and electron poor (**4d**, **4e**) aryl groups work equally well, with the exception of the 4-dimethylamino derivative (**4i**), which could not be generated.

A 5-$CF_3$-substituted oxadiazole (**5h**) was synthesized by acylation with trifluoroacetic anhydride.[88] The corresponding acyltetrazole **3h** is significantly less thermally stable with deazotation occurring at room temperature immediately after its formation. After purification by column chromatography, the

**Table 1** Optimization of the oxadiazole synthesis based on the reaction of tetrazole **2H** with *p*-toluoyl chloride[a]

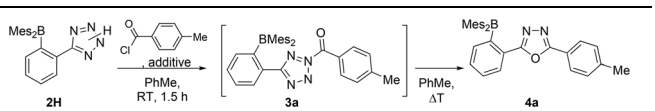


| Temperature [°C] | Additive (7 equiv.) | Isolated yield [%] |
|---|---|---|
| 90 | — | 15 |
| 110 | — | 35 |
| 130 | — | 13 |
| 110 | $NEt_3$ | 39[b] |
| 110 | $K_2CO_3$ | 95 |

[a] Solvent: toluene, acylation reaction carried out at room temperature. [b] Approximate yield, contained an unidentified impurity.

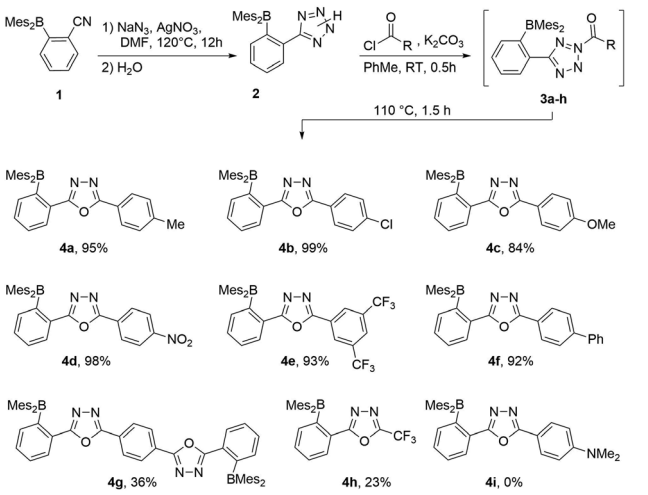


**Scheme 4** Synthesis of the borylated 1,3,4-oxadiazoles **4a** to **4h** starting from tetrazole **1**. **4i** did not form but is included in the computational survey.

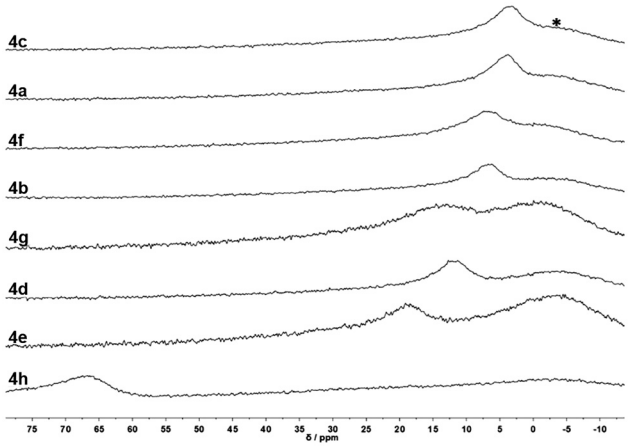


Fig. 2 $^{11}$B NMR spectra of the synthesized oxadiazoles. Recorded in either THF-$d_8$ (**4a**–**4f**, **4h**) or DCM (**4g**); * glass background signal.

$CF_3$-functionalized oxadiazole **4h** could be isolated in 23% yield.

This is immediately apparent from the $^{11}$B NMR spectra of compounds **4a** to **4f** (Fig. 2: the chemical shifts of the $^{11}$B signals correlate linearly ($R^2$ = 0.947) with the Hammett substituent parameters ($\sigma$) of the respective substituents on the phenyl ring, which can serve as measures for electron-withdrawing or electron-donating effects of the respective substituents.[57,89] **4g** and **4h** have been omitted from Fig. 3, since $\sigma$ values cannot be given for these compounds. We included DFT data for **4i** (Scheme 4), however, which could not be synthesized but was included in the computational survey.

The more electron-rich oxadiazoles exhibit the most upfield $^{11}$B chemical shifts with signals at 3.7 ppm (**4a**) and 3.2 ppm (**4c**), which are within the range of four-coordinate boron centers of the form N→$BAr_3$. Oxadiazoles with more neutral substituents exhibit slightly downfield $^{11}$B chemical shifts of 6.8 ppm (**4b**) and 6.5 ppm (**4f**), while for compounds with strongly electron-withdrawing groups **4d** (–$NO_2$) and **4e** (*m*-$CF_3$) clearly downfield-shifted $^{11}$B signals are observed at 11.8 ppm (**4d**) and 18.6 ppm (**4e**), respectively. The latter values fall into the range of N-alkylated phenyltetrazoles[59] for which labile N→B-coordination was established. Oxadiazole **4g** is only marginally soluble in THF but shows an $^{11}$B chemical shift of 13.1 ppm in DCM, in the same range as **4b** and **4e**. Compound **4h** exhibits the most downfield $^{11}$B chemical shift of 67.1 ppm among the synthesized oxadiazoles. A value in this range suggests a purely three-coordinate boron center like $Mes_3B$ (79.0 [90] ppm) or $BPh_3$ (60.2 [91] ppm).[70] Therefore, N→B interactions do not occur in **4h**.

Single crystals suitable for X-ray diffraction analysis were obtained for oxadiazoles **4a**, **4b**, **4c**, and **4f**. The crystals were grown either by diffusion of *n*-pentane into THF solutions or by slow evaporation of THF solutions. The structures show that all four compounds adopt ***closed*** N→B-coordinated geometries in the solid state (see Fig. 4). As a result, the π systems are almost planarized with torsion angles between the oxadiazole and the $PhBMes_2$ unit of 4.5° (**4a**), 5.1° (**4b**), 3.8° (**4c**) and 5.6° (**4f**). Curiously, unlike the $^{11}$B chemical shift, the experimental bond lengths do not correlate with the substituents on the phenyl ring. With respect to the N→B bond lengths, **4a** (1.642(3) Å) and **4b** (1.642(2) Å) form comparatively shorter bonds, while those in **4c** (1.667(5) Å) and **4f** (1.671(2) Å) are significantly longer. The bond lengths in **4a** and **4b** are comparable to those in *N*-benzyl-tetrazole-derivative $\mathbf{6}_{1,5}$ (1.643(8) Å, Chart 1),[59] while those in **4c** and **4f** are far longer than the N→B-bonds in the structurally closely related triazole-based boranes **5a** (1.632(2) Å), **5d** (1.638(4) Å) and **5i** (1.630(3) Å).[57] This broad variation stands in contrast to the bond lengths in the computed structures, which correlate very well with the Hammett parameter $\sigma$ (see "◆" in Fig. 3, $R^2$ = 0.957). At first glance this correlation in itself might just be a reflection of a systemic error. However, for the structurally closely related type 5 boranes[57] linear correlations (see Table 2, see also

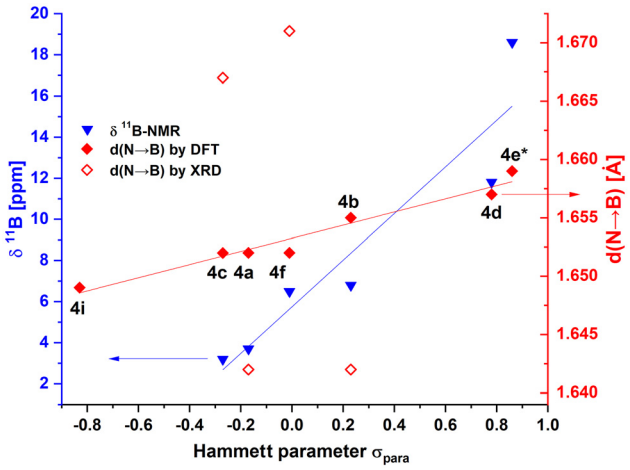


Fig. 3 Correlation between Hammett parameters and experimental $^{11}$B NMR chemical shifts (▼) and N→B-bond lengths derived using DFT (◆) and experimental X-ray diffraction (◇). * **4e**: $\sigma = 2 \times \sigma_m(CF_3) = 0.86$.

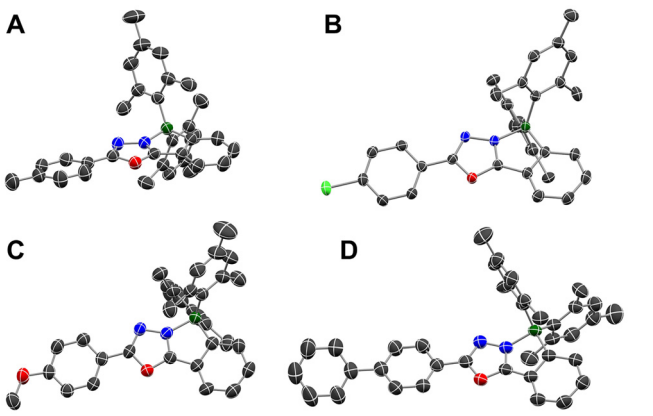


Fig. 4 Crystal structures of oxadiazoles **4a** (A), **4b** (B), **4c** (C) and **4f** (D); ellipsoids are shown with 50% probability; hydrogen atoms have not been shown for clarity.

**Table 2** Experimental and computed properties of the synthesized boranes and reference compounds

| # | Compound | R on the Ph ring | $\sigma^a$ | $^{11}$B-NMR[b] [ppm] | N→B bond lengths in oxadiazoles | | N→B bond lengths in 1,2,3-triazoles[f] | | $\Delta G_{open/closed}$[e,f] | | FIA[e,g] [kJ mol$^{-1}$] | |
|---|---|---|---|---|---|---|---|---|---|---|---|---|
| | | | | | XRD[c] [Å] | DFT[d,e] [Å] | XRD[c] [Å] | DFT[d,e] [Å] | Neutral[f] [kJ mol$^{-1}$] | Anions[f] [kJ mol$^{-1}$] | *Vs.* ***open*** [kJ mol$^{-1}$] | *Vs.* ***closed*** [kJ mol$^{-1}$] |
| 1 | **4a** | 4-Me | −0.17 | 3.7 | 1.642(3) | 1.652 | 1.632(2) | 1.668 | +4.9 | −8.3 | 307.4 | 302.5 |
| 2 | **4b** | 4-Cl | 0.23 | 6.8 | 1.642(2) | 1.655 | | 1.671 | −4.7 | −3.4 | 317.2 | 321.8 |
| 3 | **4c** | 4-OMe | −0.27 | 3.2 | 1.667(5) | 1.652 | | 1.668 | +1.8 | −8.2 | 306.9 | 305.1 |
| 4 | **4d** | 4-$NO_2$ | 0.78 | 11.8 | — | 1.657 | 1.638(4) | 1.678 | +4.4 | 45.3 | 363.9 | 359.5 |
| 5 | **4e** | 3,5-$(CF_3)_2$ | 0.86 | 18.6 | — | 1.659 | | 1.678 | −18.3 | 28.4 | 326.8 | 345.1 |
| 6 | **4f** | 4-Ph | −0.01 | 6.5 | ***closed*** | **1.652** | | | **−7.0** | **−7.7** | 313.0 | 314.3 |
| 7 | **4g** | n.a.[h] | n.a. | 13.1[i] | — | 1.656 | | | −5.3[j]/−11.6[k] | −69.86[l]/+101.3[m] | 348.0[n] | 353.3[o] |
| 8 | **4h** | $CF_3$[h] | n.a. | 67.1 | — | 1.667 | | | −12.5 | −5.3 | 318.8 | 331.2 |
| 9 | **4i**[p] | 4-$NMe_2$ | −0.83 | — | | 1.649 | 1.630(3) | 1.676 | +7.4 | −13.7 | 301.5 | 294.1 |
| 10 | $Mes_3B$[p] | | | 79.0 (ref. 90) | | | | | | | 287.7 | |
| 11 | $Mes_2BPh$[p] | | | 79.5 (ref. 90) | | | | | | | 301.8 | |
| 12 | $MesBPh_2$[p] | | | n.a. | | | | | | | 309.4 | |
| 13 | $BPh_3$[p] | | | 60.2 (ref. 91) | | | | | | | 331.8 | |
| 14 | $B(C_6F_5)_3$[p] | | | | | | | | | | 471.4[q] | |

[a] *para*-Hammett parameter, see ref. 89 **4e**: $\sigma = 2 \times \sigma_m(CF_3) = 0.86$. [b] Experimental $^{11}$B NMR shifts measured in THF-$d_8$. [c] Experimental N→B-bond lengths derived from crystal structures. [d] N→B-bond lengths in the simulated structures. [e] Level of theory M06-2X/TZVP. [f] $\Delta G$ of the ***open*** *vs.* ***closed*** conformations in the neutral boranes and radical anions respectively. [g] Fluoride ion affinities *vs.* both ***open*** and ***closed*** conformers. The lower FIA corresponds to the more stable conformer. See the text for details. [h] **4g**: Does not apply. **4h**: 5-$CF_3$-oxadiazolyl. See Scheme 4 for structures. [i] Recorded in $CD_2Cl_2$. [j] [***open/open***] *vs.* [***closed/closed***]. [k] [***open/open***] *vs.* [***closed/open***]. [l] $4g^{-1}$ [***open/open***] *vs.* [***closed/closed***]. [m] $4g^{-2}$ singlet, [***open/open***] *vs.* [***closed/closed***]. [n] FIA of **4g**: [(F→B)/***closed***] *vs.* [***open/open***]. [o] FIA of **4g**: [(F→B)/***closed***] *vs.* [***closed/closed***]. [p] Not synthesized. Only included in the DFT survey. [q] Ref. 43 reported 444 kJ mol$^{-1}$ for this compound using BP86/SV(P). [r] Data for triazoles adopted from ref. 57.

Fig. S58 in the SI) were found for both computed and experimental N→B-bond lengths, even though the calculations systematically overestimated the N–B-distance. We therefore tentatively attribute the large deviations to packing effects in the solid state.

The rotational barrier around the $C_{Mes}$–B bond could also be determined for compound **4a** using variable temperature NMR spectroscopy (see Fig. S17 in the SI), whereby a coalescence temperature for the aromatic mesityl signal of 242 K was observed, corresponding to $\Delta G_C = 47.7 \pm 0.3$ kJ mol$^{-1}$, which is in a range similar to those for tetrazole-based N→B-ladders.[59]

## Electrochemical properties

The electrochemical properties of the oxadiazoles were checked by cyclic voltammetry (CV) and square-wave voltammetry (SWV) (see section 2.5 in the SI). CV allowed classifying the irreversibility/reversibility of electrochemical reduction processes, while the first peak potentials observed in the SWV served to calculate the energies of the lowest unoccupied molecular orbitals (LUMOs) ($E_p^{red}$; see Fig. S40 and S47 in the SI). The acceptor substituted compounds **4d**, **4e**, **4g** and **4h** exhibit higher electron affinities than the parent borane **1** ($E_p^{red}$ = −2.22 V *vs.* FcH/FcH$^+$, $E_{LUMO}$ = −2.88 eV), with **4d** showing the highest electron affinity at −1.38 V ($E_{LUMO}$ = −3.72 eV). Boranes with electron-rich (**4a** and **4c**) or neutral (**4b** and **4f**) substituents provide electron affinities that are lower than or comparable to that of borane **1**, respectively.

All oxadiazoles show only irreversible reductions (see Fig. S39), with the exceptions of **4e** and **4g**, which show quasi-reversible reductions at −1.99 V and −1.84 V (*vs.* FcH/FcH$^+$), respectively. Only one reduction could be observed for compounds **4a**, **4c**, **4g** and **4h**. These reduction events are presumed to involve the empty p-orbital on boron.[57,58] For the other oxadiazoles, between two (**4b**, **4e**, **4f**) and four reductions (**4d**) were detected. The two-fold reduction of **4b** may be caused by electrochemical dechlorination[92] and subsequent reduction of the defunctionalized borane, whereas the two-fold reduction of **4e** and **4f** is deemed to be a combination of reduction at the boron center and injection of an electron into the 5-aryl-oxadiazole π-system. The first reduction of **4d** (−1.38 V *vs.* FcH/FcH$^+$) is likely associated with a redox process centered on the nitro group since the potential is in the typical range of nitro-arenes.[93] The origin of the other processes is unclear but may involve reduction at the boron center, injection of electrons into the 5-aryl-oxadiazole π-system or reductive degradation of the nitro group.

## Optical and electronic properties

To characterize the optical properties of the boranes, absorption and fluorescence spectra were recorded in DCM solution (see Fig. 5A and B). All boranes exhibit absorption maxima between 292 and 325 nm accompanied by a shoulder band towards longer wavelengths. The underlying longest wavelength absorption band ($\lambda_{max}$) that gives rise to the shoulder was derived for all compounds by Gaussian deconvolution of the experimental spectra (see Table 3 and Fig. S3–S10 in the

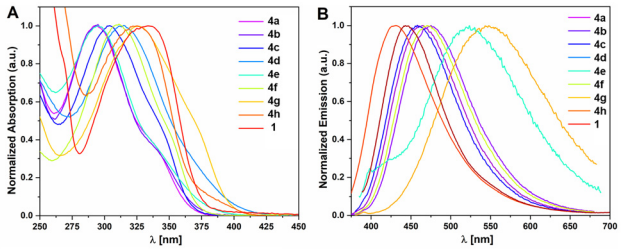


Fig. 5 UV-vis absorption (A) and fluorescence (B) spectra of the oxadiazoles. Recorded in DCM.

SI). Its intensity relative to the main band varies significantly. We were able to conclude that $\lambda_{max}$ is associated with electronic transitions involving the empty $p_z$-orbital on boron in ***open***, non-N→B-coordinated conformers, as it is suppressed in the presence of strong nucleophiles (see below). An exception to this is **4d** wherein the strongly accepting $NO_2$ group rather than the $BMes_2$ group dominates the optical properties. **4h** shows the lowest energy $\lambda_{max}$ (385 nm/3.25 V) followed by **4g** (369 nm/3.36 eV) and **4d** (362 nm/3.43 eV), while the remaining boranes show values within ±0.05 eV of the parent borane **1** (346 nm, 3.58 eV), with the notable exception of the more electron rich **4a** (338 nm/3.67 nm).

With the exception of the $NO_2$-functionalized oxadiazole **4d**, all oxadiazoles synthesized here exhibit fluorescence with emission maxima between 430 nm (**4h**) and 544 nm (**4g**). Compounds **4a** through **4g** show quantum yields of 33–35% with large Stokes shifts between 6480 $cm^{-1}$ (**4a**) and 6542 $cm^{-1}$ (**4e**). **4h** constitutes an exception with a $\Phi$ value of 4% and a much smaller Stokes shift of 2922 $cm^{-1}$. The latter may be readily explained by the smaller molecular size of **4h**, which consequently allows for less charge redistribution upon excitation.

## Anion binding

Tricoordinate boron centers can bind various nucleophiles such as fluoride or cyanide anions.[57,59,70,80] To investigate the influence of anion binding on the optical properties in more detail, absorption and emission spectra were recorded after the addition of an excess of tetrabutylammonium fluoride (TBAF) and tetrabutylammonium cyanide (TBACN) as fluoride and cyanide sources, respectively (see Fig. 6). With the exception of oxadiazole **4d**, all oxadiazoles in the survey show a blue shift in the absorption that corresponds to a suppression of the $\lambda_{max}$ band. We attribute this to the binding of the anions to the boron center, because the empty $p_z$-orbital contributes strongly to the LUMO of all ***open***-conformers except **4d-*open*** (see Fig. S51 to S53 in the SI). The LUMO is bound to participate in the lowest energy excitation. Consequently, binding of nucleophiles makes this electronic transition inaccessible. This is corroborated by experimental data on **4d**: here, the main absorption band is suppressed in the presence of anions, but the onset remains unaffected. Orbital plots show that the $p_z$-orbital contributes only to the LUMO+1 of **4d-*open***. Binding of nucleophiles is therefore expected to affect a higher energy transition, not the $\lambda_{max}$-band.

The nature of the anion does not seem to have a significant influence on the absorption properties of the oxadiazoles, as can be deduced from the very similar spectra of the fluoride- and cyanide-bound oxadiazoles.

Table 3 Summary of the optoelectronic properties of oxadiazoles **4a–4h**

| Compound | $E_p^{red}$ [a,b] [V] | LUMO[c] [eV] | $\lambda_{max}$ [d] [nm] | $\lambda_{onset}$ [nm] | $E_g^{opt}$ [e] [eV] | $\lambda_{em}$ [nm] | Stokes shift[f] [$cm^{-1}$] | $\Phi$[g] [%] |
|---|---|---|---|---|---|---|---|---|
| CN | −2.22r | −2.88 | 346 | 385 | 3.22 | 446 | 6480 | |
| **4a** | −2.41i | −2.70 | 338 | 367 | 3.38 | 463 | 7988 | 34 |
| **4b** | −2.25i | −2.85 | 342 | 372 | 3.33 | 475 | 8187 | 33 |
| | −2.36i | | | | | | | |
| **4c** | −2.43i | −2.67 | 345 | 366 | 3.39 | 459 | 7199 | 34 |
| **4d** | −1.38qr | −3.72 | 362 | 380 | 3.26 | — | — | — |
| | −1.63qr | | | | | | | |
| | −1.90i | | | | | | | |
| | −2.37i | | | | | | | |
| **4e** | −1.96r | −3.14 | 348 | 378 | 3.28 | 521 | 9542 | n.d. |
| | −2.56i | | | | | | | |
| **4f** | −2.24i | −2.86 | 349 | 371 | 3.34 | 470 | 7377 | 35 |
| | −2.81i | | | | | | | |
| **4g** | −1.85r | −3.25 | 369 | 397 | 3.12 | 544 | 8718 | n.d. |
| **4h** | −2.09i | −3.01 | 382 | 408 | 3.04 | 430 | 2922 | 4 |
| **5a**[i] | −2.64r | −2.46 | 330 | 360 | 3.44 | 380 | 3990 | 1 |
| **5c**[h] | −2.63r | −2.47 | 350 | 379 | 3.27 | 384 | 2530 | 2 |
| **5d**[h] | −1.52r | −3.58 | 360 | 417 | 2.97 | — | — | n.d. |
| **5e**[h] | −2.19r | −2.91 | 330 | 386 | 3.21 | — | — | n.d. |
| **6a**[i] | −2.58 | | 314 | 352 | 3.52 | 444 | 9325 | 93 |
| **6b**[i] | −2.66 | | 337 | 353 | 3.51 | n.d. | — | — |

[a] Peak-potential determined *via* square-wave-voltammetry in THF with 0.1 M [N*n*Bu$_4$][PF$_6$], scan speed 0.1 V $s^{-1}$. [b] Ir-/reversibility determined *via* cyclic voltammetry, scan speed 0.2 V $s^{-1}$. [c] Relative to the LUMO energy of ferrocene (−5.1 eV).[94] [d] Derived by deconvolution. See section 2.3 of the SI. [e] Derived from $\lambda_{onset}$. [f] Derived from $\lambda_{max}$ and $\lambda_{em}$. [g] Measured with an Ulbricht-integrating sphere. [h] Data adopted from ref. 57. [i] Data adopted from ref. 59.

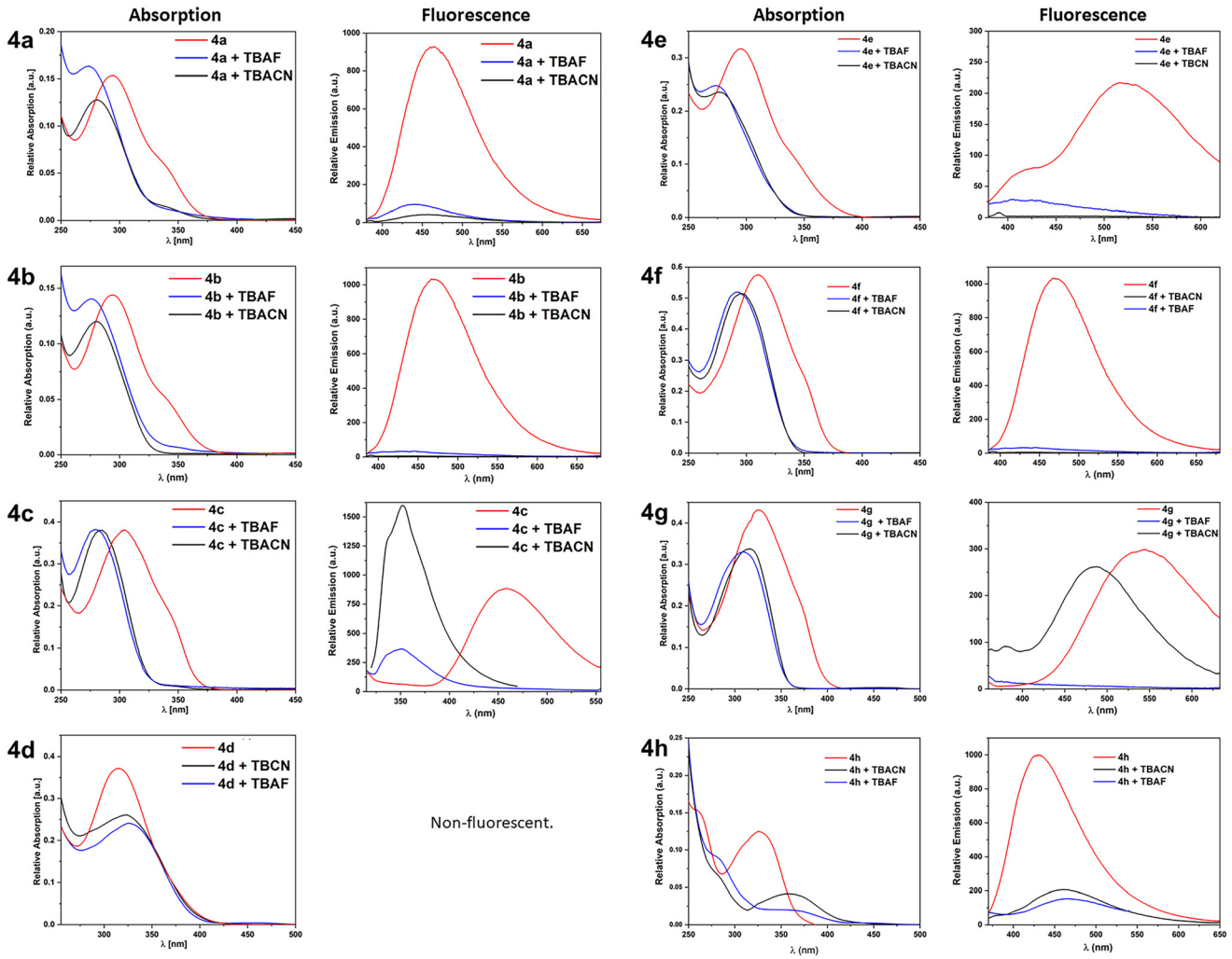


**Fig. 6** Normalized absorption and emission spectra of the synthesized oxadiazoles without and with the addition of an excess of TBAF or TBACN. Recorded in DCM.

The situation is somewhat different with regard to the fluorescence behavior. For most compounds (**4a**, **4b**, **4e**, **4f** and **4h**), the fluorescence intensity is partially (**4a**, **4e**, and **4h**) or fully suppressed regardless of the involved nucleophile (see Fig. 6).

In contrast, in the case of the OMe-substituted oxadiazole **4c**, the addition of TBAF and TBACN leads to a blue shift of the emission from 459 nm to 351 nm (see Fig. 6). However, while TBAF effects a partial suppression of the emission, addition of TBACN leads to a significant increase in emission. The most interesting behavior has been observed for **4g**: here, complete fluorescence quenching is observed upon addition of TBAF, whereas a blue shift of the emission from 544 nm to 486 nm occurs upon addition of TBACN (see Fig. 6). This means that oxadiazoles **4c** and **4g** are generally suitable to serve as fluorescence-based anion sensors. For **4c** the fluorescence spectra of the pristine borane and of the $F^{-1}$-saturated species (**4c-F**) form an isosbestic point at 395 nm, while the emission intensity after addition of TBACN is more intense at this wavelength. Consequently, selective detection at this wavelength allows discrimination between $CN^-$ and $F^-$. A similar approach is possible for **4g**. Below 504 nm the fluorescence of **4g-CN** is more intense than that of **4g**, while $F^-$-addition quenches the emission altogether. At *ca.* 408 nm the residual fluorescence of **4g** and **4g-F** reaches barely above the background, while the emission from **4g-CN** is significantly more intense.

**Comparison of triazole- and tetrazole-N→B-systems.** Previously published triazole-based boranes either included two $Mes_2B$ functionalities[58] or bore an electron-donating methoxy substituent on the borylated ring (**5a**, **5c–e**, 'type 5', Chart 1B),[57] while tetrazoles were invariably equipped with non-conjugated substituents on the heterocycle ($\mathbf{6}_{2,5}/\mathbf{6}_{1,5}$, 'type 6', Chart 1C). Direct comparisons therefore need to be approached with caution. Type **4** systems show higher electron affinities ($E_p^{red}$) than type 5 and type 6 systems. However, for type 5 systems this may be due to the Ome group, which is not directly conjugated to the $Mes_2B$ group but nevertheless

donates electrons to the π-system as a whole. For *N*-alkyl-substituted type 6-boranes, no equivalent exists in the current dataset. The optical gaps of type 4 and type **5** boranes are comparable and thus do not reflect a more effective conjugation. Again, this may be due to a donor–acceptor interaction between the Ome group and the electron poor triazole ring. Type 4 boranes exhibit larger Stokes shifts ($\mathbf{4_a}$ *vs.* $\mathbf{5_a}$ and $\mathbf{4_c}$ *vs.* $\mathbf{5_c}$), which points towards more pronounced intramolecular charge redistribution or conformational changes but this is not the case.

## Computational studies

**Structure and conformation.** In addition to the experimental studies, DFT simulations of the oxadiazoles were carried out. The geometry-optimized molecular structures show N→B bond lengths between 1.652 Å (**4c**) and 1.667 Å (**4h**), which are longer than the simulated bond lengths of the phenylpyridines (1.646 Å–1.649 Å[80]). Oxadiazoles with electron-donating substituents show shorter N→B bond lengths (**4a**: 1.652 Å, **4c**: 1.652 Å, **4f**: 1.652 Å) than compounds with electron-withdrawing substituents (**4d**: 1.657 Å, **4e**: 1.659 Å, **4h**: 1.667 Å). These results are consistent with the experimental $^{11}$B chemical shifts, which suggest a higher electron density at the boron center for the more electron-rich substituents.

Furthermore, we compared the energies of the ***open*** and ***closed*** N→B-coordinated conformers. The correlation of the Gibbs free energies indicates that the substituents on the oxadiazole regulate whether a ***closed*** N→B-coordination is favored over an ***open*** conformation (see Table 2). Boranes bearing strong acceptors (**4d**: $\Delta G_{o/c}$ = −11.8 kJ mol$^{-1}$, **4e**: −18.3 kJ mol$^{-1}$, **4h**: −12.5 kJ mol$^{-1}$) favor the ***open*** conformations. This may be attributed to the lower basicity of the oxadiazole-nitrogen due to the electron withdrawing functional groups. The reduced energetic gain from the N→B coordination cannot overcome the increased steric crowding around the tetrahedral boron center. Donor-substituted oxadiazoles (**4a**: $\Delta G_{o/c}$ = +4.9 kJ mol$^{-1}$, **4c**: +1.8 kJ mol$^{-1}$, **4i**: +7.4 kJ mol$^{-1}$) slightly favor the ***closed*** conformation. The effect is not large, however, and lies within a range of thermally accessible states at ambient temperature. The ***open*** and ***closed*** conformers of all compounds can therefore exist in dynamic equilibrium.

The conformers of the compounds introduced herein cover a slightly broader energetic range of about 25 kJ mol$^{-1}$ (+7 kJ mol$^{-1}$ to −18 kJ mol$^{-1}$) – comparable to similarly labile N→B coordinating tetrazolyl-[59] (+2 to −16 kJ mol$^{-1}$) and triazolyl-functionalized[57,58] (0 to −20 kJ mol$^{-1}$) boranes. This may be due to the more direct conjugation to the functional group but could equally be caused by subtle differences in the coordination chemistry of oxadiazoles.

**Radical anions.** To link the molecular structures with the electrochemical properties, we also modelled radical anions of the ***open*** and ***closed*** conformers (Table 2). This study showed the almost exactly inverse correlation as the neutral boranes: in the reduced state, systems with strong acceptors ($\mathbf{4d^{-1}}$, $\mathbf{4e^{-1}}$) strongly favor the ***closed*** conformation. This can be explained by a comparison of the lowest unoccupied orbitals (LUMOs) of the neutral boranes (see Fig. S48–S51 in the SI) and the spin density plots (SDPs) of the radical anions (see Fig. S53 and S54 in the SI): both the LUMOs and SDPs of the ***open*** conformers generally show strong contributions from the empty $p_z$-orbital on boron, whereas the ***closed*** conformers exhibit extended delocalization throughout the planarized π-system. The electron rich or neutral systems (**4a**, **4b** **4c**, **4f**, **4i**) slightly favor ***open*$^{-1}$*** (−3.4 to −13.7 kJ mol$^{-1}$) in rough correlation with the donor strength of the functional group. Therefore, interaction with the electron rich donor-substituted π-system is avoided. In contrast, the presence of strong acceptors (**4d**, +45.3 kJ mol$^{-1}$; **4e**, +28.4 kJ mol$^{-1}$) strongly favors ***closed*** conformers wherein the interaction between the functional group and the π-system seems maximized.

The situation is somewhat special in the diborylated **4g**. The neutral borane slightly favors a ***closed*/*open*** (−5.3 kJ mol$^{-1}$) or ***open*/*open*** (−11.6 kJ mol$^{-1}$) conformation over a ***closed*/*closed*** arrangement. This trend is amplified in the radical anion $\mathbf{4g^{-1}}$ (−69.9 kJ mol$^{-1}$) which in the ***open*/*open*$^{-1}$*** conformation benefits from stabilization by one empty $p_z$ orbital and delocalization across both oxadiazole rings in the wider π-system. In contrast, for the singlet dianion $\mathbf{4g^{-2}}$ the ***open*/*open*$^{-2}$***-conformation is strongly disfavored (+101.3 kJ mol$^{-1}$). While the HOMOs of both the ***open*/*open*$^{-2}$*** and the ***closed*/*closed*$^{-2}$***-conformers involve delocalization across the whole π-system (see Fig. S52 in the SI), the ***closed*/*closed*$^{-2}$*** conformation shows an evidently more effective conjugation across the planarized ring system.

Compared to other N→B-compounds, the range of energetic de-/stabilization of the ***closed*** conformers is broader for the oxadiazoles investigated herein compared to tetrazoles (**2**, Scheme 2[59]) but much weaker than in pyridine-based compounds.[80]

**Origin of optical properties.** To elucidate the origin of the optical properties of the boranes, time-dependent DFT (TDDFT) calculations were performed at the M06-2X/Def2-TZVP level with the PCM solvent model and dichloromethane as the solvent. The obtained electronic transition allowed the generation of UV-vis-absorption spectra that are in qualitative agreement with the experimental data (see Fig. S55 and S56 and Tables S6 and S7 in the SI). According to the calculations, the lowest energy transitions in ***open*** conformers generally involve a charge transfer from an electron rich π-orbital (HOMO or HOMO−1) towards the empty $p_z$-orbital on boron, which generally dominates the LUMO except when the very strongly electron-withdrawing –$NO_2$ group is present (**4d**). In that case, the $p_z$-orbital contributes to LUMO+1.

The HOMO and HOMO−1 tend to be delocalized across the mesityl rings attached to boron, unless strong donors like –$NMe_2$ (**4i**), –OMe (**4c**) or –Ph (**4f**) are present. Presumably, the very electron poor oxadiazole ring also lowers the frontier orbital energies of the π-system across the conjugated neighboring phenyl rings and thereby leaves the more electron rich mesityl rings to dominate the highest occupied orbitals. This effect is partially compensated for by donor–acceptor conjugation in **4i**, **4c** and **4f**. Because of the very limited spatial

 

overlap, the intensity of this transition – as indicated by the oscillator strength $f$ – is expected to be very low ($f$ = 0.036 (**4i**) to 0.125 (**4d**)).

The lowest energy transitions in ***closed*** conformers always involve a charge transfer from the mesityl groups towards π*-orbitals delocalized across the Ph-oxadiazole–Ph-π-system Apparently, the stronger +I-effect of the tetrahedral boron center makes the Mes groups much more electron rich. Only the strong donor –$NMe_2$ leads to marginal conjugation across the Ph-oxadiazole–Ph-π-system in its HOMO.

The lowest energy transitions in most ***open*** conformers are 0.1 to 0.24 eV lower in energy than in ***closed*** ones, but electronic coupling seems more efficient in ***closed*** conformations, with $f$ being between 2× (**4e**) and 34× (**4i**) higher than those in the corresponding ***open*** conformers. This corroborates the assumption that the longest-wavelength shoulder band in the absorption spectra originates from the ***open*** conformers.

**Fluoride ion affinity (FIA).** To further assess the Lewis acidity of the individual boranes, the fluoride-ion affinities (FIAs) were calculated at the M06-2X/TZVP level in the gas phase according to the following model reaction (see Table 2 for results).

$$[\text{Borane}] + F^{-1} \rightarrow [\text{Borane–F}]^{-1} \quad (1)$$

Included in the survey were the oxadiazole-containing boranes **4a** through **4i**, along with $Mes_3B$, $Mes_2BPh$, $MesBPh_2$, $BPh_3$, and $B(C_6F_5)_3$ to provide a frame of reference. For boranes **4a** through **4i**, the FIAs – expressed as $-\Delta G$ of the model reaction in kJ $mol^{-1}$ –were computed for both ***open*** and ***closed*** forms. For the subsequent discussion the lowest FIA of the two is considered the most relevant because it represents the transition between the most stable neutral conformer and the $[\text{Borane–F}]^{-1}$-complex.

The four reference boranes cover an FIA range from 287.7 kJ $mol^{-1}$ for $Mes_3B$ to 331.8 kJ $mol^{-1}$ for $BPh_3$ and 471.4 kJ $mol^{-1}$ for $B(C_6F_5)_3$. From $Mes_3B$ to $BPh_3$ the Lewis acidity increases because the Mes groups are successively replaced by the less sterically shielding and less electron rich phenyl rings. Still, $BPh_3$ is rated as only moderately Lewis-acidic, while $B(C_6F_5)_3$ is a benchmark for strong Lewis acids.

The FIAs of the synthesized boranes cover a range from 302.5 J $mol^{-1}$ (**4a**) to 359.5 kJ $mol^{-1}$ (**4d**). Borane **4i**, which could not be accessed *via* the described route, gave a lower FIA of 294.1 kJ $mol^{-1}$.

To put these results into perspective, while **4a–4h** can be regarded as more sterically crowded than $Mes_2BPh$, they all exhibit FIAs equal to (**4a**) or higher than that of this reference compound. The FIAs of the acceptor substituted **4d** (359.5 kJ $mol^{-1}$) and the bifunctional **4g** (345.1 kJ $mol^{-1}$) even exceed the FIA of $BPh_3$. While even **4d** and **4g** must still be regarded as only moderately Lewis-acidic, these results indicate that the chemical transformation reported herein allows incrementally varying the Lewis acidity of a given borane precursor over a very broad range, even in the presence of other highly sterically shielding substituents on boron.

# Conclusion

In summary, we reported the conversion of a tetrazolyl-functionalized borane precursor into a series of eight boranes bearing oxadiazolyl groups with chemically and electronically diverse substituents. The molecular structure allows for intramolecular N→B coordination and provides full conjugation between the boron center and the peripheral substituents.

A full characterization study of the optical, electrochemical and electronic properties, both experimentally and by DFT calculations, showed that the borane exhibits dynamic N→B coordination with ***open*** and ***closed*** conformers of most boranes existing in dynamic equilibrium. $^{11}B$ NMR indicates that only systems with the strongest acceptor (**4h**, 5-$CF_3$-functionalized oxadiazole) exclusively adopt the ***open*** conformation.

Our most intriguing find is that the fluorescence behavior in particular varies drastically among the individual compounds in the presence of strong nucleophiles ($F^-$, $CN^-$). While differing degrees of fluorescence quenching are observed in most cases, **4c** (4-OMe-phenyl) and **4g** (bifunctional) exhibit fluorescence shifts and selective enhancement upon binding to $CN^-$.

These results show that the synthetic strategy would offer a versatile synthetic route to libraries of tailored dyes, fluorescent sensors and Lewis acids.

# Conflicts of interest

There are no conflicts of interest to declare.

# Data availability

The data that support the findings of this study are openly available in https://zenodo.org/ at https://zenodo.org/records/17866758.

Supplementary information (SI): descriptions of the materials and instruments used, detailed synthetic procedures, and additional analytical data not provided in the main article. The latter part includes NMR ($^1H$, $^{13}C$, $^{11}B$) spectra, optical spectra, electrochemical data, mass spectrometry data, and details on crystallographic data collection and computational results including optimized computed structures, orbital- and spin-density plots, and TDDFT results. See DOI: https://doi.org/10.1039/d5ob01979f.

The authors have cited additional references within the SI.[95–102]

CCDC 2514222–2514226 (**4a**, **4b**, **4c**, **4f** and **8b**) contain the supplementary crystallographic data for this paper.[103a–e]

# Acknowledgements

JS and FP thank the German Science Foundation (DFG, German Research Foundation, project number FP 2217/4-1)

and the German Chemical Industry Fund (FCI, Liebig scholarship to FP) for financial support. Prof. Orthaber thanks the Swedish Research Council (Vetenskapsrådet) for support.

## References

1 W. Zhang and Y. Jin, *Dynamic Covalent Chemistry: Principles, Reactions, and Applications*, John Wiley & Sons, Hoboken, 2017.
2 *Constitutional Dynamic Chemistry*, ed. M. Barboiu, Springer Berlin Heidelberg, Berlin, Heidelberg, 2012, vol. 322.
3 A. J. M. Miller, Controlling ligand binding for tunable and switchable catalysis: cation-modulated hemilability in pincer-crown ether ligands, *Dalton Trans.*, 2017, **46**, 11987–12000.
4 S. E. Angell, C. W. Rogers, Y. Zhang, M. O. Wolf and W. E. Jones, Hemilabile coordination complexes for sensing applications, *Coord. Chem. Rev.*, 2006, **250**, 1829–1841.
5 T. Baumgartner and F. Jäkle, *Main Group Strategies towards Functional Hybrid Materials*, John Wiley & Sons, 2008.
6 A. Doshi and F. Jäkle, in *Comprehensive Inorganic Chemistry II*, Elsevier, 2013, pp. 861–891.
7 Y. Ren and F. Jäkle, Merging thiophene with boron: new building blocks for conjugated materials, *Dalton Trans.*, 2016, **45**, 13996–14007.
8 F. Jäkle, Topics in Organometallic Chemistry, in *Synthesis and Application of Organoboron Compounds*. ed. E. Fernández and A. Whiting, Springer, Cham, 2015, vol. 49, pp. 297–325.
9 F. Jäkle, Lewis acidic organoboron polymers, *Coord. Chem. Rev.*, 2006, **250**, 1107–1121.
10 F. Jäkle, Advances in the Synthesis of Organoborane Polymers for Optical, Electronic, and Sensory Applications, *Chem. Rev.*, 2010, **110**, 3985–4022.
11 F. Jäkle, in *Encyclopedia of Inorganic Chemistry*, ed. R. B. King, Wiley & Sons Ltd, 2005.
12 C. D. Entwistle and T. B. Marder, Applications of Three-Coordinate Organoboron Compounds and Polymers in Optoelectronics, *Chem. Mater.*, 2004, **16**, 4574–4585.
13 C. D. Entwistle and T. B. Marder, Die Borchemie leuchtet: optische Eigenschaften von MolekÃ¼len und Polymeren, *Angew. Chem.*, 2002, **114**, 3051.
14 D. Shimoyama and F. Jäkle, Controlling the aggregation and assembly of boron–containing molecular and polymeric materials, *Aggregate*, 2022, **3**(2), e149.
15 E. A. Patrick and W. E. Piers, Twenty-five years of bis-pentafluorophenyl borane: a versatile reagent for catalyst and materials synthesis, *Chem. Commun.*, 2020, **56**, 841–853.
16 E. von Grotthuss, A. John, T. Kaese and M. Wagner, Doping Polycyclic Aromatics with Boron for Superior Performance in Materials Science and Catalysis, *Asian J. Org. Chem.*, 2018, **7**, 37–53.
17 L. Ji, S. Griesbeck and T. B. Marder, Recent developments in and perspectives on three-coordinate boron materials: a bright future, *Chem. Sci.*, 2017, **8**, 846–863.
18 X. Long, J. Yao, F. Cheng, C. Dou and Y. Xia, Double B←N bridged bipyridine-containing polymer acceptors with enhanced electron mobility for all-polymer solar cells, *Mater. Chem. Front.*, 2019, **3**, 70–77.
19 X. Long, Z. Ding, C. Dou, J. Liu and L. Wang, A double B←N bridged bipyridine (BNBP)-based polymer electron acceptor: all-polymer solar cells with a high donor : acceptor blend ratio, *Mater. Chem. Front.*, 2017, **1**, 852–858.
20 R. Zhao, C. Dou, Z. Xie, J. Liu and L. Wang, Polymer Acceptor Based on B←N Units with Enhanced Electron Mobility for Efficient All–Polymer Solar Cells, *Angew. Chem., Int. Ed.*, 2016, **55**, 5313–5317.
21 X. Long, Y. Gao, H. Tian, C. Dou, D. Yan, Y. Geng, J. Liu and L. Wang, Electron-transporting polymers based on a double B←N bridged bipyridine (BNBP) unit, *Chem. Commun.*, 2017, **53**, 1649–1652.
22 X. Long, Z. Ding, C. Dou, J. Zhang, J. Liu and L. Wang, Polymer Acceptor Based on Double B←N Bridged Bipyridine (BNBP) Unit for High–Efficiency All–Polymer Solar Cells, *Adv. Mater.*, 2016, **28**, 6504–6508.
23 C. Dou, J. Liu and L. Wang, Conjugated polymers containing B←N unit as electron acceptors for all-polymer solar cells, *Sci. China: Chem.*, 2017, **60**, 450–459.
24 M. Grandl, J. Schepper, S. Maity, A. Peukert, E. Von Hauff and F. Pammer, N→B Ladder Polymers Prepared by Postfunctionalization: Tuning of Electron Affinity and Evaluation as Acceptors in All-Polymer Solar Cells, *Macromolecules*, 2019, **52**, 1013–1024.
25 M. Vanga, A. Sahoo, R. A. Lalancette and F. Jäkle, Linear Extension of Anthracene via B←N Lewis Pair Formation: Effects on Optoelectronic Properties and Singlet O 2 Sensitization, *Angew. Chem.*, 2022, **134**, e202113075.
26 A. Wakamiya, T. Taniguchi and S. Yamaguchi, Intramolecular B–N Coordination as a Scaffold for Electron–Transporting Materials: Synthesis and Properties of Boryl–Substituted Thienylthiazoles, *Angew. Chem.*, 2006, **118**, 3242–3245.
27 D.-T. Yang, J. Radtke, S. K. Mellerup, K. Yuan, X. Wang, M. Wagner and S. Wang, One-Pot Synthesis of Brightly Fluorescent Mes2B-Functionalized Indolizine Derivatives via Cycloaddition Reactions, *Org. Lett.*, 2015, **17**, 2486–2489.
28 D. R. Levine, M. A. Siegler and J. D. Tovar, Thiophene-Fused Borepins As Directly Functionalizable Boron-Containing π-Electron Systems, *J. Am. Chem. Soc.*, 2014, **136**, 7132–7139.
29 C. Reus, S. Weidlich, M. Bolte, H.-W. Lerner and M. Wagner, C-Functionalized, Air- and Water-Stable 9,10-Dihydro-9,10-diboraanthracenes: Efficient Blue to Red Emitting Luminophores, *J. Am. Chem. Soc.*, 2013, **135**, 12892–12907.
30 A. Wakamiya, K. Mori and S. Yamaguchi, 3-Boryl–2,2′–bithiophene as a Versatile Core Skeleton for Full–Color

 

Highly Emissive Organic Solids, *Angew. Chem., Int. Ed.*, 2007, **46**, 4273–4276.

31 F. Vidal, J. McQuade, R. Lalancette and F. Jäkle, ROMP-Boranes as Moisture-Tolerant and Recyclable Lewis Acid Organocatalysts, *J. Am. Chem. Soc.*, 2020, **142**, 14427–14431.

32 H. Lin, S. Patel and F. Jäkle, Tailored Triarylborane Polymers as Supported Catalysts and Luminescent Materials, *Macromolecules*, 2020, **53**, 10601–10612.

33 T. Kushida and S. Yamaguchi, A Radical Anion of Structurally Constrained Triphenylborane, *Organometallics*, 2013, **32**, 6654–6657.

34 X. Yin, J. Chen, R. A. Lalancette, T. B. Marder and F. Jäkle, Highly Electron–Deficient and Air–Stable Conjugated Thienylboranes, *Angew. Chem.*, 2014, **126**, 9919–9923.

35 X. Yin, F. Guo, R. A. Lalancette and F. Jäkle, Luminescent Main-Chain Organoborane Polymers: Highly Robust, Electron-Deficient Poly(oligothiophene borane)s via Stille Coupling Polymerization, *Macromolecules*, 2016, **49**, 537–546.

36 V. M. Hertz, N. Ando, M. Hirai, M. Bolte, H.-W. Lerner, S. Yamaguchi and M. Wagner, Steric Shielding vs Structural Constraint in a Boron-Containing Polycyclic Aromatic Hydrocarbon, *Organometallics*, 2017, **36**, 2512–2519.

37 N. Baser-Kirazli, R. A. Lalancette and F. Jäkle, Tuning the Donor–π–Acceptor Character of Arylborane–Arylamine Macrocycles, *Organometallics*, 2021, **40**, 520–528.

38 Z. Yang, K. Yang, X. Wei, W. Liu, R. Gao, F. Jäkle, Y.-L. Loo and Y. Ren, A Multiple Excited-State Engineering of Boron-Functionalized Diazapentacene Via a Tuning of the Molecular Orbital Coupling, *J. Phys. Chem. Lett.*, 2021, **12**, 9308–9314.

39 P. Li, D. Shimoyama, N. Zhang, Y. Jia, G. Hu, C. Li, X. Yin, N. Wang, F. Jäkle and P. Chen, A New Platform of B/N–Doped Cyclophanes: Access to a π–Conjugated Block–Type B 3 N 3 Macrocycle with Strong Dipole Moment and Unique Optoelectronic Properties, *Angew. Chem., Int. Ed.*, 2022, **61**, e202200612.

40 A. F. Alahmadi, X. Yin, R. A. Lalancette and F. Jäkle, Synthesis and Structure–Property Relationships in Regioisomeric Alternating Borane–Terthiophene Polymers, *Chem. – Eur. J.*, 2022, **19**(18), e202203619.

41 I. B. Sivaev and V. I. Bregadze, Lewis acidity of boron compounds, *Coord. Chem. Rev.*, 2014, **270–271**, 75–88.

42 R. J. Mayer, N. Hampel and A. R. Ofial, Lewis Acidic Boranes, Lewis Bases, and Equilibrium Constants : A Reliable Scaffold for a Quantitative Lewis Acidity/Basicity Scale, *Angew. Chem., Int. Ed.*, 2008, **47**, 7659–7663.

43 L. O. Müller, D. Himmel, J. Stauffer, G. Steinfeld, J. Slattery, G. Santiso-Quinones, V. Brecht and I. Krossing, Simple Access to the Non–Oxidizing Lewis Superacid PhF->Al(ORF)3 RF= C(CF3)3, *Angew. Chem., Int. Ed.*, 2008, **47**, 7659–7663.

44 M. Fontani, F. Peters, W. Scherer, W. Wachter, M. Wagner and P. Zanello, Adducts of Ferrocenylboranes and Pyridine Bases: Generation of Charge-Transfer Complexes and Reversible Coordination Polymers, *Eur. J. Inorg. Chem.*, 1998, **1998**, 1453–1465.

45 A. F. Alahmadi, J. Zuo and F. Jäkle, B-N Lewis pair-fused dipyridylfluorene copolymers incorporating electron-deficient benzothiadiazole comonomers, *Polym. J.*, 2023, **55**, 433–442.

46 J. Zuo, K. Liu, J. Harrell, L. Fang, P. Piotrowiak, D. Shimoyama, R. A. Lalancette and F. Jäkle, Near–IR Emissive B–N Lewis Pair–Functionalized Anthracenes via Selective LUMO Extension in Conjugated Dimer and Polymer, *Angew. Chem., Int. Ed.*, 2024, **63**, e202411855.

47 M. Vanga, A. Sahoo, R. A. Lalancette and F. Jäkle, Linear Extension of Anthracene via B←N Lewis Pair Formation: Effects on Optoelectronic Properties and Singlet O 2 Sensitization, *Angew. Chem., Int. Ed.*, 2022, **61**, e202113075.

48 Y. Shi, Y. Zeng, P. Kucheryavy, X. Yin, K. Zhang, G. Meng, J. Chen, Q. Zhu, N. Wang, X. Zheng, F. Jäkle and P. Chen, Dynamic B/N Lewis Pairs: Insights into the Structural Variations and Photochromism via Light–Induced Fluorescence to Phosphorescence Switching, *Angew. Chem., Int. Ed.*, 2022, **61**, e202213615.

49 R. P. Nandi, J. Zuo and F. Jaekle, B-N Fused Anthracene as Functional Linker for π-Extended Viologens: Near-IR Emission and Electrochromism, *Angew. Chem.*, 2026, **138**, e21634.

50 J. Miao, Y. Wang, J. Liu and L. Wang, Organoboron molecules and polymers for organic solar cell applications, *Chem. Soc. Rev.*, 2022, **51**, 153–187.

51 S. Wang, D. Yang, J. Lu, H. Shimogawa, S. Gong, X. Wang, S. K. Mellerup, A. Wakamiya, Y. Chang, C. Yang and Z. Lu, In Situ Solid–State Generation of (BN)2-Pyrenes and Electroluminescent Devices, *Angew. Chem., Int. Ed.*, 2015, **54**, 15074–15078.

52 R. Hecht, J. Kade, D. Schmidt and A. Nowak-Król, n–Channel Organic Semiconductors Derived from Air–Stable Four–Coordinate Boron Complexes of Substituted Thienylthiazoles, *Chem. – Eur. J.*, 2017, **23**, 11620–11628.

53 M. Liu, D. Zhou, Y. B. He, Y. Fu, X. Qin, C. Miao, H. Du, B. Li, Q. H. Yang, Z. Lin, T. S. Zhao and F. Kang, Novel gel polymer electrolyte for high-performance lithium-sulfur batteries, *Nano Energy*, 2016, **22**, 278–289.

54 X. Zhang, F. Rauch, J. Niedens, R. B. da Silva, A. Friedrich, A. Nowak-Król, S. J. Garden and T. B. Marder, Electrophilic C–H Borylation of Aza[5]helicenes Leading to Bowl-Shaped Quasi-[7]Circulenes with Switchable Dynamics, *J. Am. Chem. Soc.*, 2022, **144**, 22316–22324.

55 D. Volland, J. Niedens, P. T. Geppert, M. J. Wildervanck, F. Full and A. Nowak-Król, Synthesis of a Blue–Emissive Azaborathia[9]helicene by Silicon–Boron Exchange from Unusual Atropisomeric Teraryls, *Angew. Chem., Int. Ed.*, 2023, **62**(30), e20230491.

56 F. Full, Q. Wölflick, K. Radacki, H. Braunschweig and A. Nowak-Król, Enhanced Optical Properties of Azaborole Helicenes by Lateral and Helical Extension, *Chem. – Eur. J.*, 2022, **28**(62), e202202280.

57 R. Koch, Y. Sun, A. Orthaber, A. J. Pierik and F. Pammer, Turn-on fluorescence sensors based on dynamic intramolecular N→B-coordination, *Org. Chem. Front.*, 2020, **7**, 1437–1452.
58 S. Schraff, Y. Sun and F. Pammer, Tuning of electronic properties via labile N→B-coordination in conjugated organoboranes, *J. Mater. Chem. C*, 2017, **5**, 1730–1741.
59 J. Schepper, A. Orthaber and F. Pammer, Tetrazole–Functionalized Organoboranes Exhibiting Dynamic Intramolecular N→B–Coordination and Cyanide–Selective Anion Binding, *Chem. – Eur. J.*, 2024, **30**, e202401466.
60 J. Chen, R. A. Lalancette and F. Jäkle, Chiral Organoborane Lewis Pairs Derived from Pyridylferrocene, *Chem. – Eur. J.*, 2014, **20**, 9120–9129.
61 S. Schwendemann, R. Fröhlich, G. Kehr and G. Erker, Intramolecular frustrated N/B Lewis pairs by enamine hydroboration, *Chem. Sci.*, 2011, **2**, 1842.
62 G.-Q. Chen, F. Türkyilmaz, C. G. Daniliuc, C. Bannwarth, S. Grimme, G. Kehr and G. Erker, Enamine/butadienylborane cycloaddition in the frustrated Lewis pair regime, *Org. Biomol. Chem.*, 2015, **13**, 10477–10486.
63 C. Zeng, K. Yuan, N. Wang, T. Peng, G. Wu and S. Wang, The opposite and amplifying effect of B ← N coordination on photophysical properties of regioisomers with an unsymmetrical backbone, *Chem. Sci.*, 2019, **10**, 1724–1734.
64 Y. Cao, J. K. Nagle, M. O. Wolf and B. O. Patrick, Tunable Luminescence of Bithiophene-Based Flexible Lewis Pairs, *J. Am. Chem. Soc.*, 2015, **137**, 4888–4891.
65 Y. Cao, N. E. Arsenault, D. Hean and M. O. Wolf, Fluorescence Switching of Intramolecular Lewis Acid–Base Pairs on a Flexible Backbone, *J. Org. Chem.*, 2019, **84**, 5394–5403.
66 C. T. Hoang, I. Prokes, G. J. Clarkson, M. J. Rowland, J. H. R. Tucker, M. Shipman and T. R. Walsh, Study of boron–nitrogen dative bonds using azetidine inversion dynamics, *Chem. Commun.*, 2013, **49**, 2509.
67 S. J. Cassidy, I. Brettell-Adams, L. E. McNamara, M. F. Smith, M. Bautista, H. Cao, M. Vasiliu, D. L. Gerlach, F. Qu, N. I. Hammer, D. A. Dixon and P. A. Rupar, Boranes with Ultra-High Stokes Shift Fluorescence, *Organometallics*, 2018, **37**, 3732–3741.
68 Y. Shi, J. Wang, H. Li, G. Hu, X. Li, S. K. Mellerup, N. Wang, T. Peng and S. Wang, A simple multi-responsive system based on aldehyde functionalized amino-boranes, *Chem. Sci.*, 2018, **9**, 1902–1911.
69 Z. M. Hudson and S. Wang, Impact of Donor–Acceptor Geometry and Metal Chelation on Photophysical Properties and Applications of Triarylboranes, *Acc. Chem. Res.*, 2009, **42**, 1584–1596.
70 C. R. Wade, A. E. J. Broomsgrove, S. Aldridge and F. P. Gabbaï, Fluoride ion complexation and sensing using organoboron compounds, *Chem. Rev.*, 2010, **110**, 3958–3984.
71 N. Ishida, T. Moriya, T. Goya and M. Murakami, Synthesis of Pyridine–Borane Complexes via Electrophilic Aromatic Borylation, *J. Org. Chem.*, 2010, **75**, 8709–8712.
72 S. A. Iqbal, J. Pahl, K. Yuan and M. J. Ingleson, Intramolecular (directed) electrophilic C–H borylation, *Chem. Soc. Rev.*, 2020, **49**, 4564–4591.
73 M. Grandl, B. Rudolf, Y. Sun, D. F. Bechtel, A. J. Pierik and F. Pammer, Intramolecular N→B Coordination as a Stabilizing Scaffold for π-Conjugated Radical Anions with Tunable Redox Potentials, *Organometallics*, 2017, **36**, 2527–2535.
74 M. Grandl, Y. Sun and F. Pammer, Generation of an N→B Ladder-type Structure by Regioselective Hydroboration of an Alkenyl-Functionalized Quaterpyridine, *Chem. – Eur. J.*, 2016, **22**, 3976–3980.
75 M. Grandl, T. Kaese, A. Krautsieder, Y. Sun and F. Pammer, Hydroboration as an Efficient Tool for the Preparation of Electronically and Structurally Diverse N→B-Heterocycles, *Chem. – Eur. J.*, 2016, **22**, 14373–14382.
76 M. Grandl, Y. Sun and F. Pammer, Electronic and structural properties of N→B-ladder boranes with high electron affinity, *Org. Chem. Front.*, 2018, **5**, 336–352.
77 F. Pammer, J. Schepper, J. Glöckler, Y. Sun and A. Orthaber, Expansion of the scope of alkylboryl-bridged N→B-ladder boranes: New substituents and alternative substrates, *Dalton Trans.*, 2019, **48**, 10298–10312.
78 M. Grandl and F. Pammer, Preparation of Head-to-Tail Regioregular 6-(1-Alkenyl)-Functionalized Poly(pyridine-2,5-diyl) and its Post-Functionalization via Hydroboration, *Macromol. Chem. Phys.*, 2015, **216**, 2249–2262.
79 K. Yuan, N. Suzuki, S. K. Mellerup, X. Wang, S. Yamaguchi and S. Wang, Pyridyl Directed Catalyst-Free trans -Hydroboration of Internal Alkynes, *Org. Lett.*, 2016, **18**, 720–723.
80 J. D. W. Schepper, A. Orthaber and F. Pammer, Preparation of Structurally and Electronically Diverse N→B-Ladder Boranes by [2 + 2 + 2] Cycloaddition, *J. Org. Chem.*, 2021, **86**, 14767–14776.
81 B. Reichart and C. O. Kappe, High-temperature continuous flow synthesis of 1,3,4-oxadiazoles via N-acylation of 5-substituted tetrazoles, *Tetrahedron Lett.*, 2012, **53**, 952–955.
82 R. Huisgen, J. Sauer and H. J. Sturm, Acylierung 5-substituierter Tetrazole zu 1.3.4-Oxdiazolen, *Angew. Chem.*, 1958, **9**, 272–273.
83 V. K. Gour, S. Yahya and M. Shahar Yar, Unveiling the chemistry of 1,3,4-oxadiazoles and thiadiazols: A comprehensive review, *Arch. Pharm.*, 2023, **357**, 2300328.
84 J. Lu, I. Persson, H. Lind, J. Palisaitis, M. Li, Y. Li, K. Chen, J. Zhou, S. Du, Z. Chai, Z. Huang, L. Hultman, P. Eklund, J. Rosen, Q. Huang and P. O. Å. Persson, Tin+1Cn MXenes with fully saturated and thermally stable Cl terminations, *Nanoscale Adv.*, 2019, **1**, 3680–3685.
85 U. Mitschke and P. Bäuerle, The electroluminescence of organic materials, *J. Mater. Chem.*, 2000, **10**, 1471–1507.
86 R. Deng, L. Li, M. Song, S. Zhao, L. Zhou and S. Yao, Synthesis and optoelectronic properties of oxadiazole coordinated boron complexes, *CrystEngComm*, 2016, **18**, 4382–4387.
87 D. Zhou, D. Liu, X. Gong, H. Ma, G. Qian, S. Gong, G. Xie, W. Zhu and Y. Wang, Solution-Processed Highly Efficient

 

Bluish-Green Thermally Activated Delayed Fluorescence Emitter Bearing an Asymmetric Oxadiazole–Difluoroboron Double Acceptor, *ACS Appl. Mater. Interfaces*, 2019, **11**, 24339–24348.

88 L. I. Vereshchagin, O. N. Verkhozina, F. A. Pokatilov and V. N. Kizhnyaev, Synthesis of 2-Substituted 5-Trifluoromethyl-1, 3, 4-oxadiazoles, *Russ. J. Org. Chem.*, 2007, **43**, 1575–1576.

89 C. Hansch, A. Leo and R. W. Taft, A Survey of Hammett Substituent Constants and Resonance and Field Parameters, *Chem. Rev.*, 1991, **91**, 165–195.

90 N. M. D. Brown, F. Davidson and J. W. Wilson, Dimesitylboryl compounds, *J. Organomet. Chem.*, 1981, **209**, 1–11.

91 C. D. Good and D. M. Ritter, Alkenylboranes. II. Improved Preparative Methods and New Observations on Methylvinylboranes, *J. Am. Chem. Soc.*, 1962, **84**, 1162–1166.

92 N. Hoshi, K. Sasaki, S. Hashimoto and Y. Hori, Electrochemical dechlorination of chlorobenzene with a mediator on various metal electrodes, *J. Electroanal. Chem.*, 2004, **568**, 267–271.

93 H. Jung, R. H. Heflich, P. P. Fu, A. U. Shaikh and P. E. Hartman, Nitro group orientation, reduction potential, and direct–acting mutagenicity of nitro–polycyclic aromatic hydrocarbons, *Environ. Mol. Mutagen.*, 1991, **17**, 169–180.

94 C. M. Cardona, W. Li, A. E. Kaifer, D. Stockdale and G. C. Bazan, Electrochemical Considerations for Determining Absolute Frontier Orbital Energy Levels of Conjugated Polymers for Solar Cell Applications, *Adv. Mater.*, 2011, **23**, 2367–2371.

95 W. L. Armarego and D. D. Perrin, *Purification of laboratory chemicals*, Butterworth-Heinemann, Oxford, 4th edn, 1997.

96 G. R. Fulmer, A. J. M. Miller, N. H. Sherden, H. E. Gottlieb, A. Nudelman, B. M. Stoltz, J. E. Bercaw and K. I. Goldberg, NMR Chemical Shifts of Trace Impurities: Common Laboratory Solvents, Organics, and Gases in Deuterated Solvents Relevant to the Organometallic Chemist, *Organometallics*, 2010, **29**, 2176–2179.

97 S. Ando and T. Matsuura, Substituent shielding parameters of fluorine–19 NMR on polyfluoroaromatic compounds dissolved in dimethyl sulphoxide– d 6, *Magn. Reson. Chem.*, 1995, **33**, 639–645.

98 P. Mani, A. K. Singh and S. K. Awasthi, AgNO3 catalyzed synthesis of 5-substituted-1H-tetrazole via [3 + 2] cycloaddition of nitriles and sodium azide. Dedicated to the memory of late Dr. Tarkeshwar Gupta, *Tetrahedron Lett.*, 2014, **55**, 1879–1882.

99 I. V. Bliznets, A. A. Vasil'ev, S. V. Shorshnev, A. E. Stepanov and S. M. Lukyanov, Microwave-assisted synthesis of sterically hindered 3-(5-tetrazolyl) pyridines, *Tetrahedron Lett.*, 2004, **45**, 2571–2573.

100 B. Akhlaghinia and S. Rezazadeh, A Novel Approach for the Synthesis of 5-Substituted-1, *J. Braz. Chem. Soc.*, 2012, **23**, 2197–2203.

101 B. Du, X. Jiang and P. Sun, Palladium-Catalyzed Highly Selective ortho -Halogenation (I, Br, Cl) of Arylnitriles via sp 2 C–H Bond Activation Using Cyano as Directing Group, *J. Org. Chem.*, 2013, **78**, 2786–2791.

102 G. M. Sheldrick, A short history of SHELX, *Acta Crystallogr., Sect. A: Found. Crystallogr.*, 2008, **64**, 112–122.

103 (*a*) CCDC 2514222: Experimental Crystal Structure Determination, 2026, DOI: 10.5517/ccdc.csd.cc2qd7yb; (*b*) CCDC 2514223: Experimental Crystal Structure Determination, 2026, DOI: 10.5517/ccdc.csd.cc2qd7zc; (*c*) CCDC 2514224: Experimental Crystal Structure Determination, 2026, DOI: 10.5517/ccdc.csd.cc2qd80f; (*d*) CCDC 2514225: Experimental Crystal Structure Determination, 2026, DOI: 10.5517/ccdc.csd.cc2qd81g; (*e*) CCDC 2514226: Experimental Crystal Structure Determination, 2026, DOI: 10.5517/ccdc.csd.cc2qd82h.